frontiers | Frontiers in Materials

TYPE Original Research
PUBLISHED 17 October 2023
DOI 10.3389/fmats.2023.1287623

OPEN ACCESS

EDITED BY
Liang Ren,
Dalian University of Technology, China

REVIEWED BY
Congrui Grace Jin,
University of Nebraska-Lincoln,
United States
王 Wang,
Zhejiang Sci-Tech University, China
Qiang Xu,
Dalian University of Technology, China

*CORRESPONDENCE
Tong Jiang,
jiangtong@ncwu.edu.cn

RECEIVED 02 September 2023
ACCEPTED 04 October 2023
PUBLISHED 17 October 2023

CITATION
Pan X, Wan L, Jiang T, Jia Y and Zhang S (2023), Experimental study on strength and failure characteristics of mortar specimens with prefabricated cracks under uniaxial and triaxial stress. *Front. Mater.* 10:1287623. doi: 10.3389/fmats.2023.1287623

Experimental study on strength and failure characteristics of mortar specimens with prefabricated cracks under uniaxial and triaxial stress

Xuwei Pan, Li Wan, Tong Jiang*, Yanchang Jia and Shuo Zhang

College of Geosciences and Engineering, North China University of Water Resources and Electric Power, Zhengzhou, Henan, China

Cracks in rock masses have adverse effects on their mechanical characteristics and the stability of rock mass engineering. For this experiment, uniaxial compression and true triaxial compression unloading tests were conducted on mortar specimens. The strength of the specimens was the lowest when the dip angle of the crack was 45°. Under uniaxial compression, the failure mode was mainly tensile failure. With an increase in the crack dip angle of the specimens, the types of cracks changed from shear to tensile cracks. Under true triaxial compression, the confining pressure considerably increased the strength and deformation characteristics of the specimens and weakened the influence of the crack dip angle on the strength. The failure mode when the crack dip angle was 15° was mainly tensile. The failure mode when the crack dip angles were 45° and 75° was mainly tensile–shear composite. With the increase in the crack dip angle, the failure degree of the specimens was more severe. Under the triaxial unloading confining, the failure mode was mainly shear. Compared with uniaxial compression, the failure degree of the specimens was more severe under true triaxial compression and true triaxial unloading. The innovation of this experiment is the use of a special mold to prepare specimens. We recommend that scholars conduct experimental and numerical simulation studies on different crack geometries.

KEYWORDS

failure mode and crack propagation, prefabricated cracks, strength and failure characteristics, types of generated cracks, uniaxial and triaxial stress

1 Introduction

After experiencing a long geological evolution and human disturbances, the original joints of rock masses expand and connect to form macroscopic cracks. The development and expansion of cracks in a rock mass play a decisive role in the mechanical behavior of the rock mass, which seriously affects the stability and safety of many rockmass engineering (such as mining, underground space, slope, civil engineering, etc.). Therefore, to increase the feasibility and stability of geotechnical engineering, scholars must study the evolution process of cracks in rock masses, the failure mode of fractured rock masses, and the influence of cracks on the mechanical properties of rock masses.

Research has been conducted on crack propagation evolution in fractured rock masses. Chen et al. (2022) studied the influence of the prefabricated crack size on the directional propagation

law of rock type-I cracks. Xu et al. (2021) studied the crack closure and propagation modes of rock specimens containing a single crack under bidirectional shear testing. Yang and Jiang (2010) analyzed the influence of the fracture length and dip angle on crack propagation mechanisms in brittle sandstone. Lee and Jeon (2011) noted that the cracks of specimens with prefabricated cracks need to undergo evolution, such as initiation, propagation, and penetration. Ashby and Sammis (1990) established a failure model of crack growth, which considered the interaction between cracks. The influence of different fracture depths and fracture dip angles on the penetration mechanism of prefabricated cracks was analyzed by Shen and Stephansson (1993). Bobet and Einstein (1998) (Shen et al., 1995; Wong et al., 2001a) studied the initiation, propagation, and penetration mechanism of secondary cracks. Dyskin et al. (2003) studied the crack propagation law of specimens with a single inclined prefabricated crack. Wong et al. (2004a), Wong et al. (2004b), Wong and Einstein (2009b), and Wong et al. (2018) studied the influence of crack strikes (angles with the principal compressive stress) and crack depth on crack propagation morphology under uniaxial- and biaxial compression conditions and proposed many different types of crack propagation modes, such as shear, tensile, and tensile–shear mixed models. Nguyen et al. (2011) studied the crack propagation mechanism of tuff with intermittent cracks under a plane strain condition. Liu et al. (2014) indicated that under a low confining pressure, secondary cracks begin to expand from the tip of the original prefabricated crack with a larger initiation angle. Hao et al. (2021) studied the evolution law of strain fields in the rock bridge region, which contained granite with prefabricated cracks. Mei et al. (2020) indicated that the crack propagation rate in a mortar sample with a single prefabricated crack decreases first and then increases. Liu et al. (2018) indicated that with the increase in normal stress, the length of a single tensile crack becomes shorter and the number increases. Shen et al. (2022) indicated that the loading rate has an effect on the energy release and the generation of new cracks. Ai et al. (2019) indicated that the impact velocity has an important influence on the crack propagation process and dynamic mechanical properties. Song et al. (2019) studied the evolution of prefabricated cracks in coal and rock samples under uniaxial compression.

Research has also been conducted on the failure mode of fractured rock masses. Liu et al. (2019) studied the crack propagation and failure law of specimens with x-type cross cracks under different confining pressures. Yang et al. (2012) studied the failure characteristics of rocks with three intermittent cracks under uniaxial or biaxial compression. Wong and Chau (1998) and Wong et al. (2001b) refined the failure modes of specimens with two cracks under different confining pressures and classified the three failure modes summarized by Bobet and Einstein (1998) into nine types. Nasseri et al. (1997) and Niandou et al. (1997) analyzed the influence of the fracture dip angle on mechanical parameters and found that three different failure modes existed. Bobet (2000) indicated that under high confining pressure, only shear cracks initiate and eventually lead to specimen failure. Wong et al. (2006b) analyzed the influence of the length, dip angle, and width of prefabricated cracks on the failure mode of rocks with prefabricated cracks.

Research has also been conducted on the mechanical properties of fractured rock masses. Zhang et al. (2020) combined with the theory of frost heaving mechanics and fracture mechanics, carried out the freeze–thaw cycle test, and analyzed failure modes and mechanical characteristics of crack growth. Li et al. (2022) analyzed the influence of prefabricated crack angles on the mechanical properties and failure modes of coal samples under uniaxial compression. The geometric parameters of the joints in the rock mass (such as the occurrence, length, roughness, connectivity, filling, etc.) are the main factors that influence the mechanical characteristics of jointed rock masses. Wong and Einstein (2009a) analyzed the strength characteristics of marble with intermittent double cracks under uniaxial compression. Yang and Jing (2010) studied the influence of the length and dip angle of prefabricated cracks on crack propagation and the mechanical characteristics of rock masses.

Xi et al. (2020) indicated that crack initiation and propagation will occur when the stress is far less than the compressive strength of the rock for granite specimens with prefabricated cracks. Liu et al. (2022) proposed a mechanical model of multi-cracked rock masses and noted that the strength of multi-cracked specimens decreases first and then increases with the increase in the crack inclination angle. Tiwari and Rao (2006) studied the influence of joint morphology on strain hardening and softening and the plastic behavior of rock masses with triaxial and true triaxial compression tests. Gehle and Kutter (2003) studied the effects of the length, spacing, and inclination of cracks on the shear deformation and fracture failure process of the specimens. Prudencio and Van Sint Jan (2007) studied the effects of the spacing, inclination, and arrangement of the joints on the failure mode, strength, and deformation characteristics of rock masses.

Acoustic emission (AE) technology has been widely used when analyzing the crack propagation process (Chang and Lee, 2004; Lei et al., 2004; Tham et al., 2005; Xi et al., 2020; Shen et al., 2022). Chen et al. (2022) analyzed the response characteristics of AEs during crack propagation. Li et al. (2022) analyzed the influence of the prefabricated crack angle on the AE response of coal samples under uniaxial compression. Gao et al. (2023) monitored the mechanical behavior of red sandstone via two analyses that were conducted by using AE technology. Deng et al. (2022) analyzed the AE characteristics of prefabricated single-crack sandstone under uniaxial compression. Worley et al. (2019) demonstrated the effectiveness of AE technology when detecting cracks. Liu et al. (2021) studied the failure evolution process of intact rock and fractured rock mass specimens under uniaxial loading condition on the basis of the maximum amplitude distribution of AE events.

Wang et al. (2022) examined the mechanical properties and fracture propagation characteristics of the fractured rock mass under coupling of heavy rainfall infiltration and mining unloading by using of PFC numerical software. Xiao et al. (2022) conducted numerical simulation research on rock mechanics and fracture characteristics. Wang et al. (2023) used PFC2D to study the peak strength and failure characteristics of rock-like materials with dual prefabricated crack combinations. Liang et al. (2021) used PFC2D to conduct a numerical simulation on sandy mudstone with prefabricated cross defects under uniaxial compression. Manouchehrian et al. (2014) used PFC2D to simulate the biaxial compression test on a rock with a single crack. Na et al. (2022) carried out a series of numerical simulation experiments to investigate the creep evolution processes of simple fractured rock masses under

loading. Zhang et al. (2019) used ABAQUS to conduct a numerical simulation on the stress intensity factor at the tip of the prefabricated crack. Huang et al. (2016) used AUTODYN to simulate a triaxial test on sandstone with two cracks. Wang et al. (2014) used RFPA3D to analyze the influence of crack parameters on rock strength and failure characteristics. Xi et al. (2020) used the extended finite element method to simulate the initiation and propagation of prefabricated cracks in granite specimens. Li et al. (2022) conducted a numerical simulation on the evolution process of prefabricated crack propagation in translucent alumina ceramic sheets during flame thermal shock.

Duan et al. (2022) recorded the fracture damage behavior of prefabricated cracks by using high-speed photography. Gao and Li (2022) used a digital image correlation (DIC) to study the strain field around the crack. Jiang et al. (2019) used a DIC to study the influence of prefabricated cracks on the mechanical properties and deformation fields of specimens.

A large number of studies have shown that, the mechanical parameters of and research results obtained when using rock masses and rock-like materials are highly similar, which indicates that using rock-like materials instead of rock masses for research is feasible (Reyes and Einstein, 1991; Shen and Stephansson, 1993; Shen et al., 1995; Bobet and Einstein, 1998; Wong and Chau, 1998; Gehle and Kutter, 2003; Liu et al., 2014).

The existing research objects are mostly hard rocks, while there is relatively few research on soft rocks that are commonly in engineering. Compared to hard rock, soft rock contains a large number of joints and fractures, resulting in poor mechanical characteristics, and the fracture mechanism and fracture evolution law under compression are also different. Therefore, it is necessary to study the fracture mechanism and crack propagation evolution law of soft rock materials containing cracks under compression. The original rock of the mortar sample prepared by our research institute is the silty mudstone (belonging to soft rock) in the Huainan of China. The stress ratio of the mortar sample and the original rock is 1/3, and the Poisson's ratio, internal friction angle ratio, and cohesion ratio are 1. The results of this study will provide guidance and reference for soft rock mass engineering.

For this experiment, mortar specimens with prefabricated cracks with three dip angles were used for uniaxial compression, true triaxial compression, and true triaxial loading tests. The effects of the crack dip angle on the strength, failure mode, and crack propagation of the specimens were studied.

2 Experimental

2.1 Specimen preparation

Cement mortar was used to create specimens with prefabricated cracks. The mix ratio of cement: sand: water was 1:5:1.25. The cement was ordinary Portland cement with a mark of 32.5, and the sand was fine-grained river sand. The main indicators of cement and sand are shown in Tables 1, 2.

The specimens were cubes with a side length of 150 mm. The specimens contained a thorough prefabricated crack, which was in the middle of the specimens. The length of the crack was 150 mm, the width was 30 mm, and the thickness was 2 mm. A certain angle between the crack and the vertical direction was present, which was the crack dip angle. To study the effect of the crack dip angle on the mechanical characteristics and failure mode of the specimens, the crack dip angles were designed to be 15, 45, and 75°. The specimen model with a 45° crack dip angle is shown in Figure 1.

The mold used to prepare the specimens was a special mold (Figure 2). In total, nine prefabricated crack mortar specimens with 3 different crack angles were poured in the mold at a time. The crack simulation plate was used to reserve gaps for the cracks. The rotating wheel drove the crack simulation plates to rotate together, and this was used to set the crack dip angle.

The cement and fine sand were put into the mixer and evenly stirred, and then water was added; the mixture continued to be stirred, and then the mortar mixture was created. The prepared mortar mixture was poured into the pouring chamber in the mold. The edges and corners of the pouring chamber were fully vibrated to remove the bubbles from the mortar mixture, and then the top surface of the mortar mixture was leveled. The mortar mixture after pouring is shown in Figure 3. The mold was removed after 24 h of pouring, and the mortar specimens were taken out for standby after being put into water for curing for 28 days. The prepared specimens are shown in Figure 4.

2.2 Test method

Uniaxial compression, true triaxial compression, and true triaxial unloading tests were conducted, as shown in Figure 5. The confining pressure of the true triaxial compression and unloading test was σ_2 = 0.8 and σ_3 = 0.4 MPa, respectively. The number of repetitions for each type of test was 2.

The LYC true triaxial apparatus was used for the uniaxial compression, true triaxial compression, and true triaxial

TABLE 1 Indicators of cement.

Item	Compressive strength (Mpa)		Flexural strength (Mpa)		Setting time (h: min)		Water consumption of standard consistency (%)
	3 days	28 days	3 days	28 days	Initial setting	Final setting	
Test value	24.8	48.3	5.8	9.1	1:55	3:55	27.5

TABLE 2 Indicators of sand.

Sieve aperture/mm	9.5	4.75	2.36	1.18	0.60	0.30	0.15
Percentage of accumulated sieve residues (%)	0	5.7	22.9	36.5	62.8	80.7	94.1

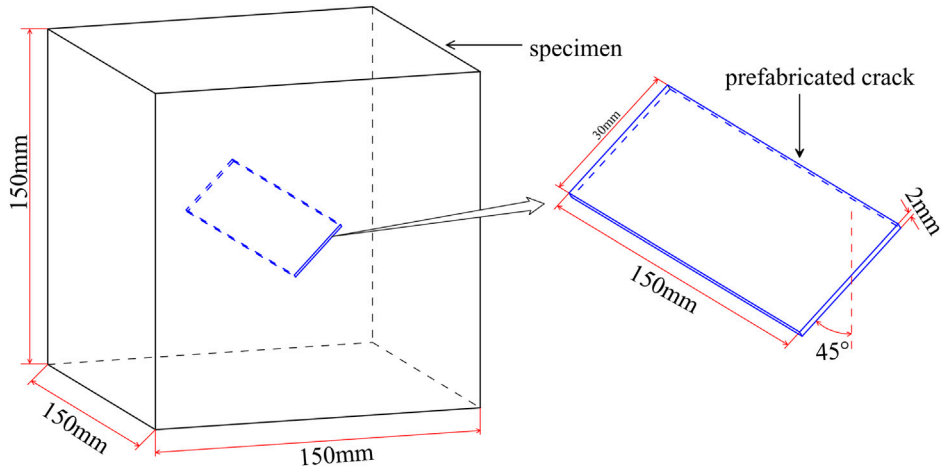

FIGURE 1
The specimen model with a 45° crack dip angle.

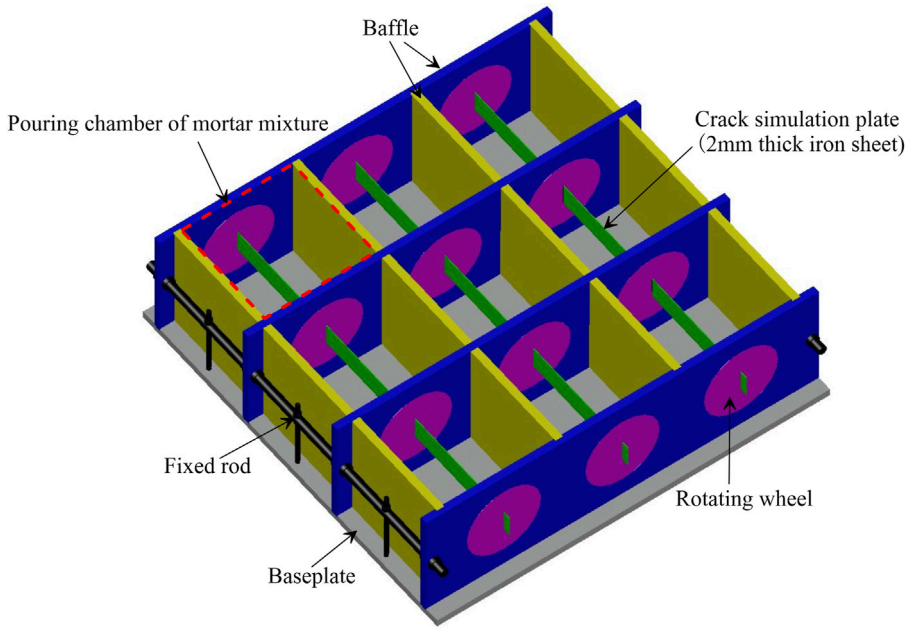

FIGURE 2
Mold for preparing specimens.

unloading test to provide axial pressure. The maximum uniaxial pressure of the instrument was 450 kN. The load and displacement sensor were used to measure the stress and deformation of the specimens, respectively. The load sensor had a range of 300 kN, and the displacement sensor measurement range was ±50 mm. Both the load sensor and the displacement sensor were connected to the DH3823 data acquisition system (sampling rate: up to 1 kHz), which collected the stress and deformation data during the test.

The uniaxial compression test is shown in Figure 6. The specimens were placed on the pressure pedestal, the steel plates were placed on the bottom and top surfaces, and the load sensor and displacement sensor were placed above the steel plates on the top surface. The rear end of the load sensor was connected to a hydraulic jack (used to provide an axial load). The vertical axes of the specimens, load sensor, and hydraulic jack coincided.

The true triaxial compression test is shown in Figure 7. The four sides and the top surface of the specimens placed on the pressure pedestal were wrapped by five pressure ends. The rear end of each pressure end was connected to a load sensor, displacement sensor, and hydraulic jack, which was used to measure the stress and deformation of the three axes of the specimens and provide three axial loads. During the loading process of the true triaxial compression test, three-dimensional stress was first applied according to the design value of

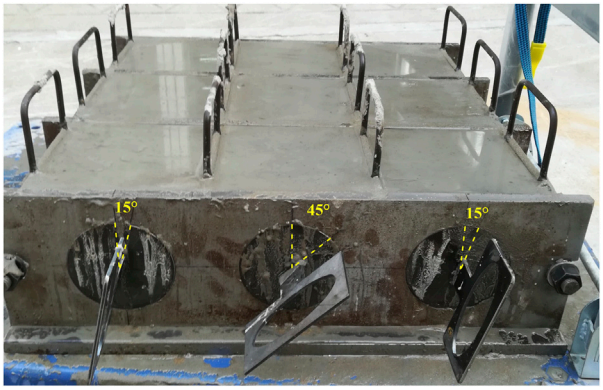

FIGURE 3
Mortar mixture after pouring.

the confining pressure, and the confining pressure was kept constant; additionally, the vertical stress was continuously loaded until the specimens failed to withstand the stress. Because the specimens were wrapped by the pressure ends, observing the test process at all times and stopping the test when the vertical stress rapidly decreased and the vertical deformation of the specimens rapidly increased was necessary.

The test preparation, loading method, and data acquisition of the true triaxial unloading test was consistent with that of the true triaxial compression test. Firstly, the triaxial stress was applied according to the design value of the confining pressure, and the confining pressure was kept constant. Secondly, the vertical stress was continuously loaded to 0.85 times of the peak stress during the true triaxial compression test, and then the minimum principal stress was unloaded. The test was stopped when the specimens rapidly deformed in the direction of the minimum principal stress.

FIGURE 4
Specimens.

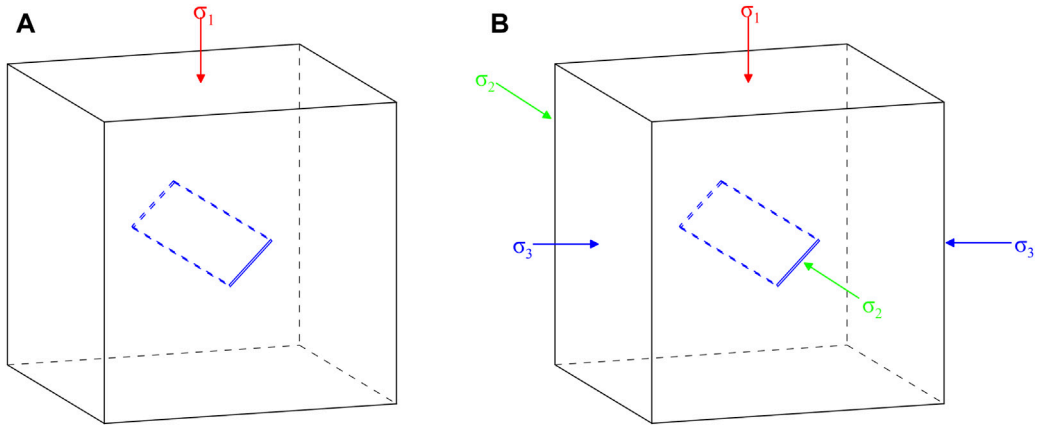

FIGURE 5
Sketch of test. **(A)** Uniaxial compression. **(B)** True triaxial compression.

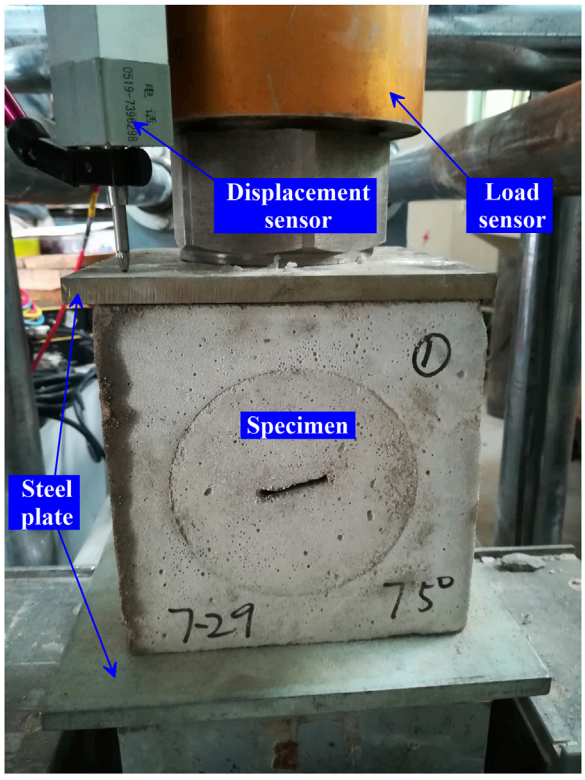

FIGURE 6
Uniaxial compression test.

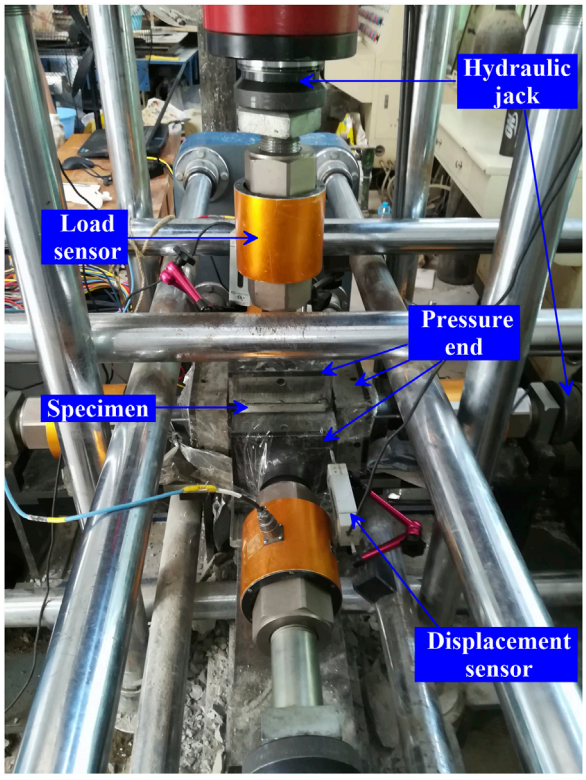

FIGURE 7
True triaxial compression and true triaxial unloading tests.

3 Test results and analyses

After the test, the data collected by the DH3823 data acquisition system were imported into the origin software. The axial stress–strain curve was drawn based on the axial stress and deformation data of the specimens, and the strength characteristics of the specimens were analyzed based on the peak stress of the specimens.

3.1 Stress–strain curve

The stress–strain curve of the specimens under uniaxial compression was divided into four stages (see Figure 8). The initial loading stage (OA) of the curve was the compaction stage, and the internal pores and microcracks of the specimens were closed under compression. The straight rising stage (AB) was the elastic deformation stage; the curve was approximate to a straight line, and

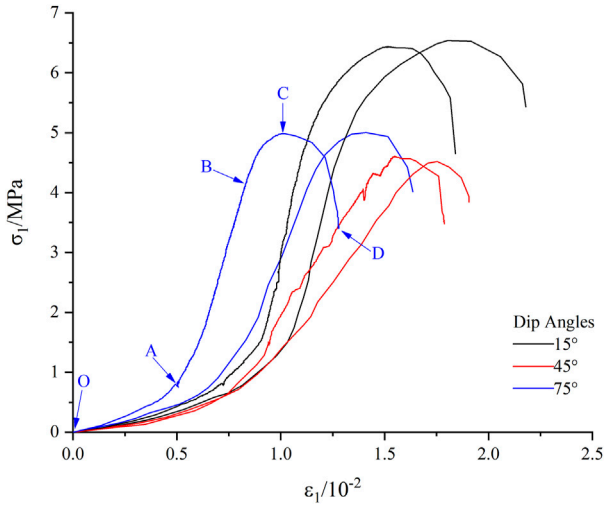

FIGURE 8
Stress–strain curve under uniaxial compression.

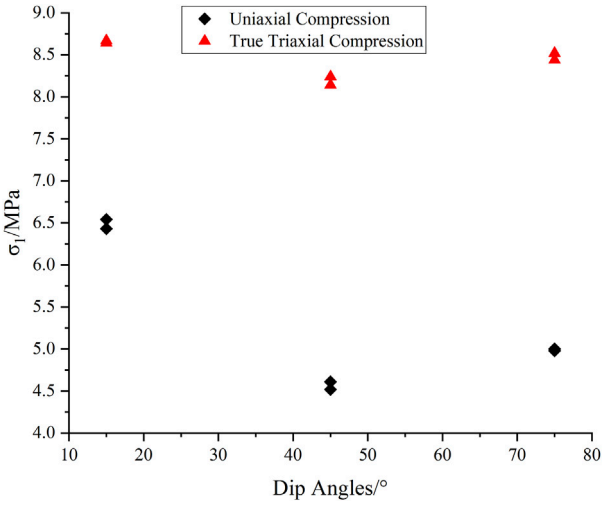

FIGURE 10
Strength.

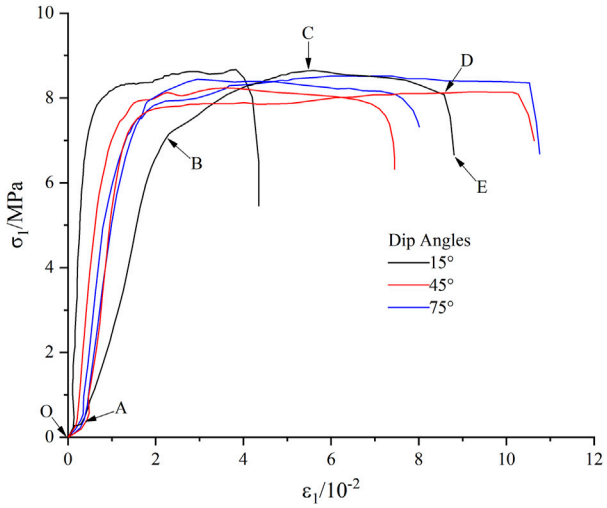

FIGURE 9
Stress–strain curve under true triaxial compression.

the stress rapidly increased with the strain. The rising stage (BC) of the curve was the plastic deformation stage, and the stress slowly increased with the strain. In the failure stage (CD), the stress of the specimens rapidly decreased after reaching the peak stress (point C), and the specimens finally failed.

The first principal stress–strain curve of the specimens under true triaxial compression (Figure 9) can be divided into five stages. Compared with the stress–strain curve under uniaxial compression, the shape of the curve during the three stages before the peak stress was similar, but the shape after the peak stress was remarkably different. After the stress reached the peak value (point C), the specimens entered the large deformation stage (CD). Because of the confining pressure, the stress slowly decreased and the strain rapidly increased in this stage. During the failure stage (DE), the stress of the specimens rapidly decreased, and the specimens finally failed.

3.2 Strength

The strength of the specimens during the uniaxial compression and true triaxial compression test is shown in Figure 10. During the uniaxial compression test, the mean value of peak stress of the specimens with crack dip angles of 15°, 45°, and 75° was 6.49, 4.57, and 4.99 MPa, respectively. During the true triaxial compression test, the mean value of peak stress of the specimens with 15°, 45°, and 75° crack dip angles were 8.66, 8.19, and 8.48 MPa, respectively. The peak stress of the specimens decreased first and then increased with the increase in the crack dip angle, whereby the minimum stress occurred with the 45° dip angle. The peak stress of the specimens with 15°, 45°, and 75° crack dip angles under true triaxial compression was 1.33, 1.79, and 1.69 times that under uniaxial compression, respectively. Under true triaxial compression, because of the confining pressure, the compaction degree of the internal pores and microcracks of the specimens was higher during the compression process, the compactness of the specimens increased, and the strength characteristics of the specimens increased. The confining pressure considerably enhanced the strength characteristics of the specimens and weakened the effect of the crack dip angle on the strength.

3.3 Failure mode and crack propagation

Wong and Einstein (2009b) classified the cracks generated by specimens containing single flaws under compression into seven types, including three types of tensile cracks, three types of shear cracks, and one type of tension–shear crack. Referring to Wong et al.'s classification of cracks generated in specimens that contained single flaws under compression, three types of cracks were generated

10.3389/fmats.2023.1287623

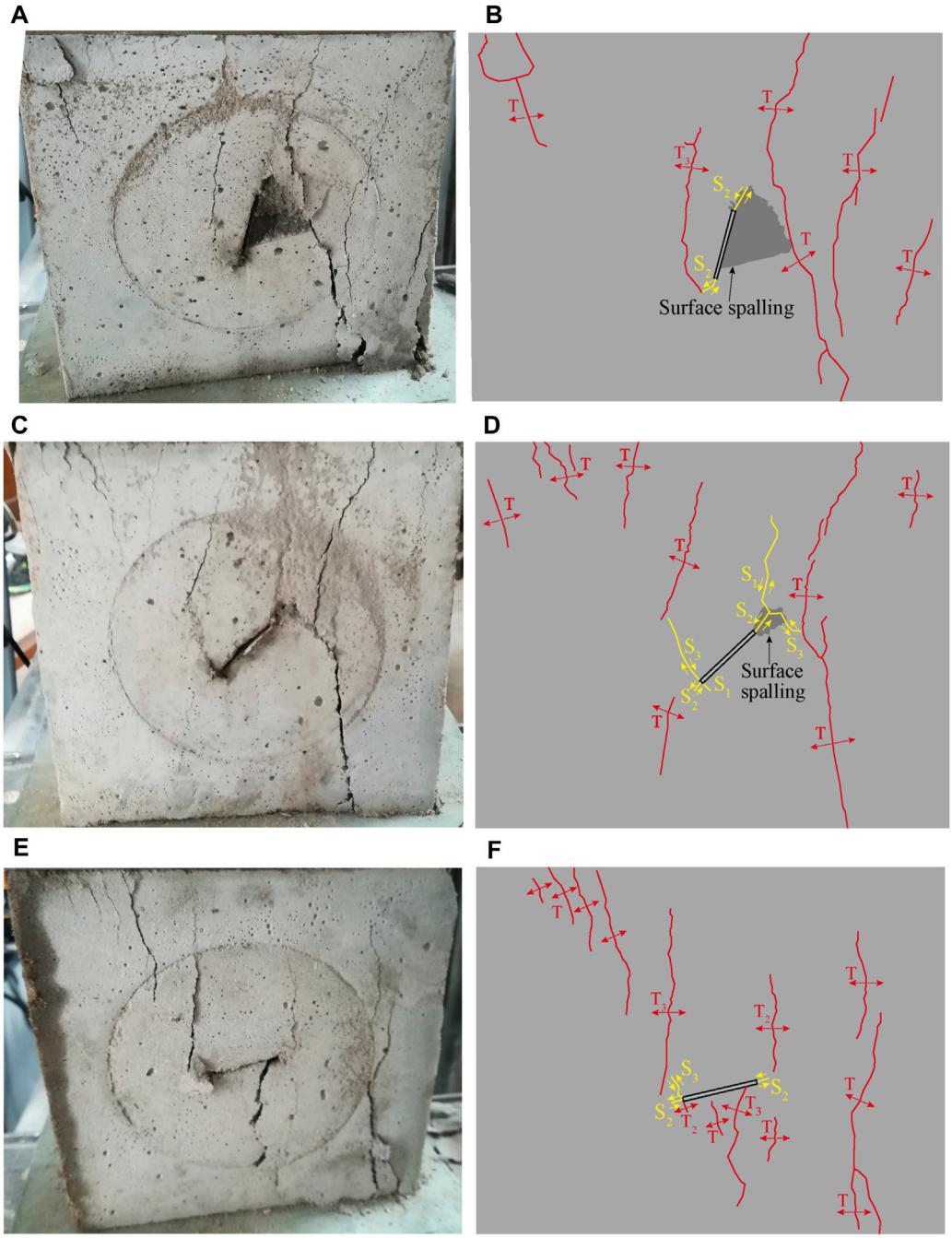

FIGURE 11
Failure of specimens under uniaxial compression. The crack dip angle is 15° **(A,B)**. The crack dip angle is 45° **(C,D)**. The crack dip angle is 75° **(E,F)**.

during this experiment: tensile (T), shear (S), and mixed tensile–shear cracks (Mc).

The failure of the specimens during the uniaxial compression test is shown in Figure 11. The failure mode of the specimens with three types of crack dip angles was mainly tensile failure, and this was accompanied by a few shear cracks. The S2 shear cracks were generated at the tip of the prefabricated crack, and the crack direction was approximately parallel to the prefabricated crack. In addition, three types of shear cracks, S1, S2, and S3, were generated in the specimens with a 45° crack dip angle, and S3 shear cracks and T, T2, and T3 tensile cracks were generated in the specimens with a 75° crack dip angle.

The failure mechanism of the specimens with cracks under uniaxial compression was analysed.

With the increase in stress during uniaxial compression, shear cracks and tensile cracks were generated at the tip of the prefabricated cracks due to the stress concentration. With the increase in the crack dip angle of the specimens, the types of cracks generated at the tip of the prefabricated crack increased and changed from shear to tensile cracks. Compared with the left

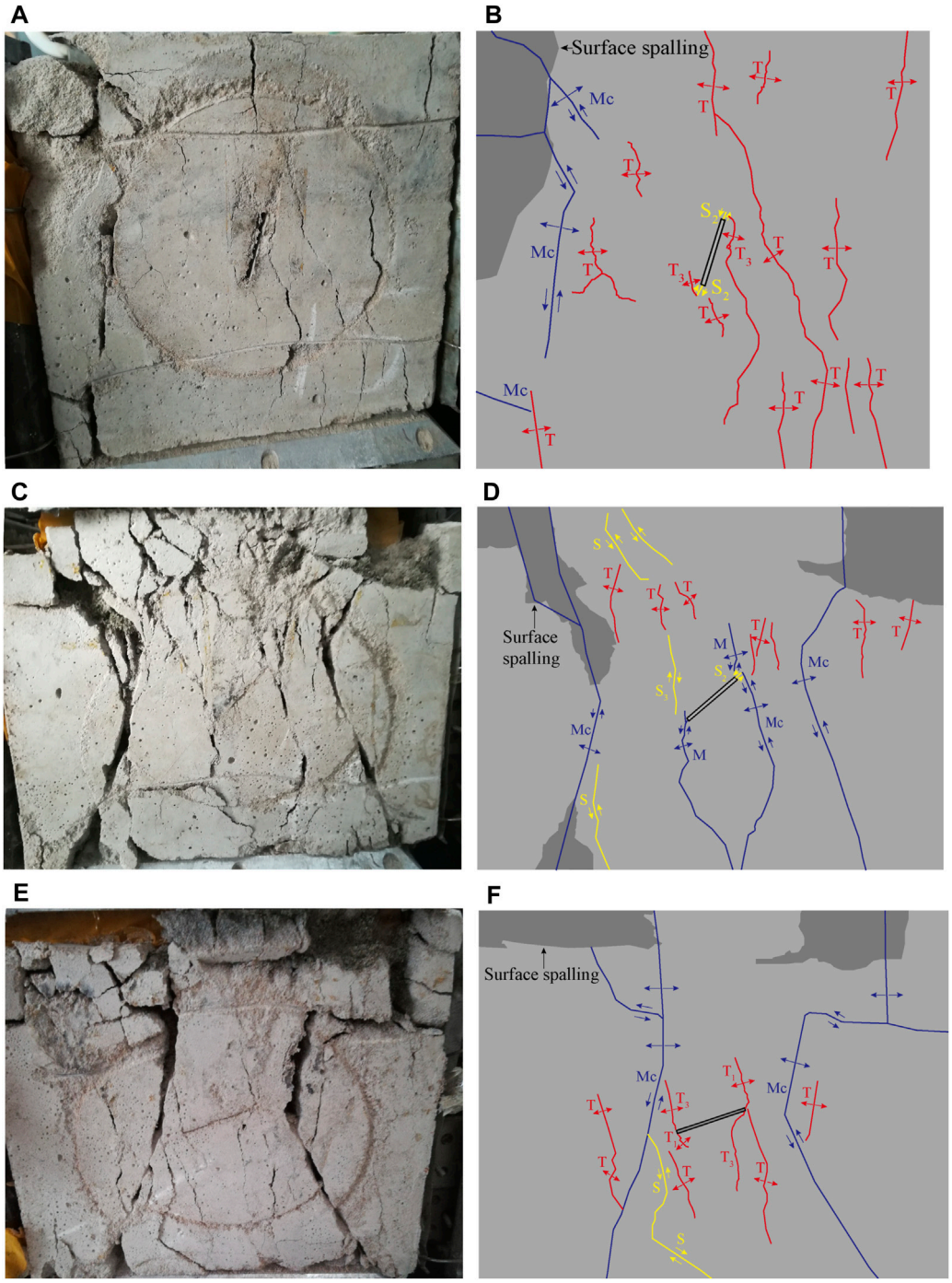

FIGURE 12
Failure of specimens under true triaxial compression. The crack dip angle is 15° **(A,B)**. The crack dip angle is 45° **(C,D)**. The crack dip angle is 75° **(E,F)**.

side of the specimens, the tip of the prefabricated crack on the right side of the specimens was closer to the loading end, and the stress concentration was higher, so the newly generated cracks were more numerous and wider, and the damage on the right side of the specimens was more serious than that on the left side.

The vertical axes of the specimens, pressure pedestal, steel plates, load sensor, and hydraulic jack were coincident, so the factor of bias pressure during loading was excluded. With the increase in the crack dip angle, the vertical height difference between the upper and lower tips of the prefabricated crack gradually decreased, the distance difference from the loading end gradually decreased, the difference in the stress concentration gradually decreased, and finally the difference in the damage degree between the left and right sides of the specimens gradually weakened.

The failure of the specimens during the true triaxial compression test is shown in Figure 12. The failure mode of the specimens with

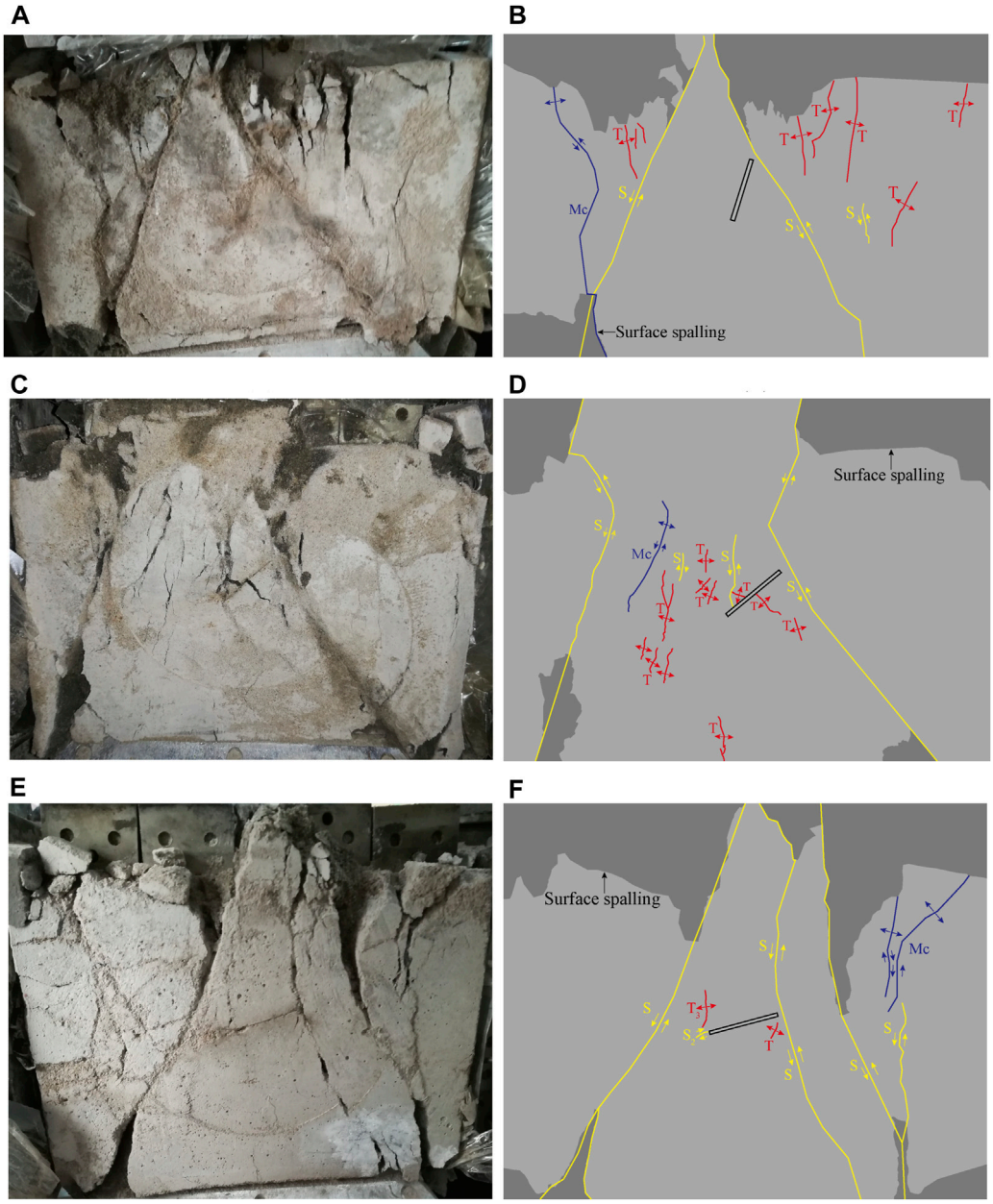

FIGURE 13
Failure of specimens under true triaxial unloading. The crack dip angle is 15° **(A,B)**. The crack dip angle is 45° **(C,D)**. The crack dip angle is 75° **(E,F)**.

15° a crack dip angle was mainly tensile and was accompanied by tensile–shear composite (Mc) and shear cracks. The failure mode of the specimens with a 45° crack dip angle was mainly tensile–shear composite (M and Mc) and was accompanied by tensile cracks and shear cracks. The failure mode of the specimens with a 75° crack dip angle was mainly tensile–shear composite (Mc) and was accompanied by tensile and shear cracks. With the increase in the crack dip angle of the specimens, the surface spalling of the specimens was more obvious, and the damage degree of the specimens was more severe. Compared with uniaxial compression, the damage degree of the specimens was more severe under true triaxial compression.

The failure of the specimens under true triaxial unloading is shown in Figure 13. The failure mode of the specimens was mainly shear and was accompanied by tensile and tensile–shear composite (Mc) cracks. No cracks were generated near the prefabricated cracks in the specimens with a 15° dip angle. Many tensile cracks and a small number of shear cracks were generated near the prefabricated cracks in the specimens with a 45° dip angle. A small number of tensile and shear cracks were generated near the prefabricated cracks in the specimens with a 75° dip angle. More than two shear cracks through the top and bottom of the specimens led to their failure. The failure degree of the specimens with a crack and a 75° dip angle was the most

serious. Compared with true triaxial compression, the deformation of the three axes of the specimens was larger under true triaxial unloading.

4 Discussion

The orientation of cracks has a significant effect on failure. The scale (width, length), quantity, inclination angle, spacing, roughness, connectivity, position, and filling of cracks have important effects on failure mode of the specimen. In this study, the location of the cracks is located in the middle of the sample, and the cracks will be set at the top and bottom of the sample in the future research work. The fillers of cracks have a significant influence on the mechanical characteristics and failure modes of materials. In future research, we will design and add gypsum with low strength as the fillers to study the specific impact of the fillers on the mechanical characteristics and failure modes.

Existing research results indicate that the presence of cracks significantly reduces the mechanical characteristics of the specimen. The scale (width, length), quantity, inclination angle, spacing, roughness, connectivity, position, and filling of cracks have important effects on the mechanical characteristics and failure mode of the specimen. The mechanical characteristics of the sample are negatively correlated with the number and scale of cracks; The strength and elastic modulus of the sample are the smallest when the crack inclination angle is 45°; The inclination angle of the crack has a significant impact on the initiation stress of the specimen; The strength and elastic modulus of the sample decrease with the increase of crack connectivity (Dyskin et al., 2003; Prudencio and Van Sint Jan, 2007; Yang and Jiang, 2010; Liu et al., 2018; Liu et al., 2019; Mei et al., 2020; Xi et al., 2020; Li et al., 2022; Liu et al., 2022; Shen et al., 2022). The research results on strength and crack propagation in this study are consistent with existing research conclusions.

The existing research objects are mostly hard rocks, while there is relatively few research on soft rocks that are commonly in engineering. Compared to hard rock, soft rock contains a large number of joints and fractures, resulting in poor mechanical characteristics, and the fracture mechanism and fracture evolution law under compression are also different. Therefore, it is necessary to study the fracture mechanism and crack propagation evolution law of soft rock materials containing cracks under compression. The original rock of the mortar sample prepared by our research institute is the silty mudstone (belonging to soft rock) in the Huainan of China.

The authors of most of the existing studies used a single mold to prepare the specimens (Wong and Chau, 1998; Wong et al., 2001b; Gehle and Kutter, 2003; Prudencio and Van Sint Jan, 2007; Wong and Einstein, 2009b; Lee and Jeon, 2011; Liu et al., 2014; Jiang et al., 2019; Liu et al., 2019), and only one specimen could be prepared at a time. Therefore, the differences between the specimens were large. The innovation of this experiment is the use of a special mold to prepare specimens; this mold can be used to prepare nine specimens at the same time, and it greatly reduces the influence of the differences in the specimens on the experimental results. The shortcomings of this experiment are the lack of SEM tests on the specimens, AEs and DICs, and numerical simulations of the test results.

5 Conclusion

Mortar specimens with prefabricated cracks and three dip angles were fabricated for uniaxial compression, true triaxial compression, and true triaxial loading tests. The effects of the crack dip angle on the strength, failure mode, and crack propagation of the specimens were studied.

The strength of the specimens was the lowest as the dip angle of 45°. Under true triaxial compression, the confining pressure remarkably enhanced the strength and deformation characteristics of the specimens and weakened the effect of the crack dip angle on the strength. Compared with the stress–strain curve when the specimens were under uniaxial compression, the shape after the peak stress was considerably different, the specimens entered into the large deformation stage, and the stress slowly decreased with the strain rapidly increased in this stage due to the confining pressure.

Under uniaxial compression, the failure mode was mainly tensile failure. With the increase in the crack dip angle, the types of cracks generated at the tip of the prefabricated crack increased and changed from shear to tensile cracks. Under true triaxial compression, the failure mode when the specimens had a 15° crack dip angle was mainly tensile. The failure mode when the specimens had 45° and 75° crack dip angles was mainly tensile–shear composite. With the increase in the crack dip angle, the damage degree of the specimens was more severe. Under the true triaxial unloading, the failure mode was mainly shear, and more than two shear cracks through the top and bottom of the specimens led to their failure.

Compared with uniaxial compression, the damage degree of the specimens was more severe under true triaxial compression and unloading.

Data availability statement

The datasets presented in this study can be found in online repositories. The names of the repository/repositories and accession number(s) can be found in the article/Supplementary Material.

Author contributions

XP: Conceptualization, Data curation, Investigation, Writing–original draft, Writing–review and editing. LW: Formal Analysis, Methodology, Writing–original draft, Writing–review and editing. TJ: Conceptualization, Supervision, Writing–review and editing. YJ: Formal Analysis, Methodology, Writing–review and editing. SZ: Formal Analysis, Funding acquisition, Writing–review and editing.

Funding

The authors declare financial support was received for the research, authorship, and/or publication of this article. This work was supported by High-level Talents Foundation of the North China University of Water Resources and Electric Power, Grant Number 202005007, Key Research and Development and Promotion Project of Henan Province in 2022 (Science and Technology Research), Grant Number 222102320463, National Natural Science Foundation of China, Grant Numbers 42107169 and 42207187, Foundation for University Key Teacher by the Ministry of Education of He-nan Province, Grant Number 2020GGJS-094, Open Fund of State Key Laboratory of Geohazard Prevention and Geoenvironment Protection, Chengdu University of Technology, Grant Number SKLGP2021K016.

Conflict of interest

The authors declare that the research was conducted in the absence of any commercial or financial relationships that could be construed as a potential conflict of interest.

Publisher's note

References

Ai, D. H., Zhao, Y. C., Xie, B., and Li, C. W. (2019). Experimental study of fracture characterizations of rocks under dynamic tension test with image processing. *SHOCK Vib.* 2019, 1–14. doi:10.1155/2019/6352609

Ashby, M. F., and Sammis, C. G. (1990). The damage mechanics of brittle solids in compression. *pure Appl. Geophys.* 133 (3), 489–521. doi:10.1007/BF00878002

Bobet, A., and Einstein, H. H. (1998). Fracture coalescence in rock-type materials under uniaxial and biaxial compression. *Int. J. Rock Mech. Min. Sci.* 35 (7), 863–888. doi:10.1016/s0148-9062(98)00005-9

Bobet, A. (2000). The initiation of secondary cracks in compression. *Eng. Fract. Mech.* 66 (2), 187–219. doi:10.1016/s0013-7944(00)00009-6

Chang, S. H., and Lee, C. I. (2004). Estimation of cracking and damage mechanisms in rock under triaxial compression by moment tensor analysis of acoustic emission. *Int. J. Rock Mech. Min. Sci.* 41 (7), 1069–1086. doi:10.1016/j.ijrmms.2004.04.006

Chen, L. X., Guo, W. Y., Zhang, D. X., and Zhao, T. B. (2022). Experimental study on the influence of prefabricated fissure size on the directional propagation law of rock type-I crack. *Int. J. ROCK Mech. Min. Sci.* 160, 105274. doi:10.1016/j.ijrmms.2022.105274

Deng, M., Zhang, Z. Z., Yu, W. J., Xin, J. L., and Xu, S. Q. (2022). Acoustic emission characteristics and damage law for prefabricated single-crack sandstone under uniaxial compression. *Struct. CONTROL HEALTH Monit.* 29 (10). doi:10.1002/stc.3018

Duan, Z., Dong, C. X., Yan, X. S., Sun, Q., and Li, B. (2022). Experimental research of fracture damage behavior of loess with different prefabricated cracks. *Eng. Fract. Mech.* 275, 108849. doi:10.1016/j.engfracmech.2022.108849

Dyskin, A. V., Sahouryeh, E., Jewell, R. J., Joer, H., and Ustinov, K. B. (2003). Influence of shape and locations of initial 3-D cracks on their growth in uniaxial compression. *Eng. Fract. Mech.* 70 (15), 2115–2136. doi:10.1016/s0013-7944(02)00240-0

Gao, A. S., Qi, C. Z., Shan, R. L., Wang, C. L., and Kocharyan, G. G. (2023). AE characteristic and mechanical behaviors of red sandstone with two prefabricated close-collinear-equal length cracks under compression. *ACS OMEGA* 8 (2), 2476–2484. doi:10.1021/acsomega.2c06951

Gao, B., and Li, Z. (2022). Study on the stress-strain relationships and deterioration modes of HTPB propellant with prefabricated cracks. *Adv. Polym. Technol.* 2022, 1–9. doi:10.1155/2022/9772946

Gehle, C., and Kutter, H. K. (2003). Breakage and shear behaviour of intermittent rock joints. *Int. J. Rock Mech. Min. Sci.* 40 (5), 687–700. doi:10.1016/s1365-1609(03)00060-1

Hao, J. W., Qiao, L., Li, Z. J., and Li, Q. W. (2021). Study on the fracture behavior of prefabricated fissures granite based on DIC and laser scanning techniques. *FATIGUE & Fract. Eng. Mater. Struct.* 44 (5), 1372–1390. doi:10.1111/ffe.13435

Huang, D., Gu, D., Yang, C., Huang, R., and Fu, G. (2016). Investigation on mechanical behaviors of sandstone with two preexisting flaws under triaxial compression. *Rock Mech. Rock Eng.* 49 (2), 375–399. doi:10.1007/s00603-015-0757-3

Jiang, T., Pan, X., Lei, J., Zhang, J., and Wang, W. (2019). Rupture and crack propagation in artificial soft rock with preexisting fractures under uniaxial compression. *Geotechnical Geol. Eng.* 37 (3), 1943–1956. doi:10.1007/s10706-018-0736-z

Lee, H., and Jeon, S. (2011). An experimental and numerical study of fracture coalescence in pre-cracked specimens under uniaxial compression. *Int. J. Solids Struct.* 48 (6), 979–999. doi:10.1016/j.ijsolstr.2010.12.001

Lei, X., Masuda, K., Nishizawa, O., Jouniaux, L., Liu, L., Ma, W., et al. (2004). Detailed analysis of acoustic emission activity during catastrophic fracture of faults in rock. *J. Struct. Geol.* 26 (2), 247–258. doi:10.1016/S0191-8141(03)00095-6

Li, Q. X., Li, Y. Q., Li, J., Li, L., Wu, X. F., Shao, Y. F., et al. (2022a). Prefabricated crack propagation in translucent alumina ceramic sheets during flame thermal shock. *Eng. Fract. Mech.* 263, 108285. doi:10.1016/j.engfracmech.2022.108285

Li, Z. H., Tian, H., Niu, Y., Wang, E. Y., Zhang, X., He, S., et al. (2022b). Study on the acoustic and thermal response characteristics of coal samples with various prefabricated crack angles during loaded failure under uniaxial compression. *J. Appl. Geophys.* 200, 104618. doi:10.1016/j.jappgeo.2022.104618

Liang, D. X., Zhang, N., Rong, H. Y., and Xiang, Z. (2021). Experimental and numerical studies on crack initiation and coalescence in sandy mudstone with prefabricated cross-flaws under uniaxial compression. *SHOCK Vib.* 2021, 1–17. doi:10.1155/2021/6672913

Liu, J., Zhu, Z., and Wang, B. (2014). The fracture characteristic of three collinear cracks under true triaxial compression. *Sci. World J.* 2014, 1–5. doi:10.1155/2014/459025

Liu, T. Y., Cui, M. Y., Li, Q., Yang, S., Yu, Z. F., Sheng, Y. S., et al. (2022). Fracture and damage evolution of multiple-fractured rock-like material subjected to compression. *MATERIALS* 15 (12), 4326. doi:10.3390/ma15124326

Liu, X., Liu, Q., Liu, B., Zhu, Y., and Zhang, P. (2019). Failure behavior for rocklike material with cross crack under biaxial compression. *J. Mater. Civ. Eng.* 31 (2), 2540. doi:10.1061/(asce)mt.1943-5533.0002540

Liu, X., Zhao, X., Zhang, S., Congyan, R., and Zhao, R. (2021). Research on the failure evolution process of rock mass base on the acoustic emission parameters. *Front. Phys.* 9, 635306. doi:10.3389/fphy.2021.635306

Liu, Y. X., Xu, J., and Zhou, G. (2018). Relation between crack propagation and internal damage in sandstone during shear failure. *J. Geophys. Eng.* 15 (5), 2104–2109. doi:10.1088/1742-2140/aac85e

Manouchehrian, A., Sharifzadeh, M., Marji, M. F., and Gholamnejad, J. (2014). A bonded particle model for analysis of the flaw orientation effect on crack propagation mechanism in brittle materials under compression. *Archives Civ. Mech. Eng.* 14 (1), 40–52. doi:10.1016/j.acme.2013.05.008

Mei, J., Yang, L., Sheng, X. C., Song, G. X., Yang, W. M., and Zhang, B. (2020). Time-dependent propagation of 3-D cracks in rocks under hydromechanical coupling. *ROCK Mech. ROCK Eng.* 53 (4), 1923–1934. doi:10.1007/s00603-019-02020-2

Na, Z., Lixin, M., Laigui, W., and Yibin, Z. (2022). Numerical simulation of creep fracture evolution in fractured rock masses. *Front. Earth Sci.* 10, 901742. doi:10.3389/feart.2022.901742

Nasseri, M. H., Rao, K. S., and Ramamurthy, T. (1997). Failure mechanism in schistose rocks. *Int. J. Rock Mech. Min. Sci.* 34 (3), 219.e1–219.e15. doi:10.1016/S1365-1609(97)00099-3

Nguyen, T. L., Hall, S. A., Vacher, P., and Viggiani, G. (2011). Fracture mechanisms in soft rock: identification and quantification of evolving displacement discontinuities by extended digital image correlation. *Tectonophysics* 503 (1), 117–128. doi:10.1016/j.tecto.2010.09.024

Niandou, H., Shao, J. F., Henry, J. P., and Fourmaintraux, D. (1997). Laboratory investigation of the mechanical behaviour of Tournemire shale. *Int. J. Rock Mech. Min. Sci.* 34 (1), 3–16. doi:10.1016/S1365-1609(97)80029-9

Prudencio, M., and Van Sint Jan, M. (2007). Strength and failure modes of rock mass models with non-persistent joints. *Int. J. Rock Mech. Min. Sci.* 44 (6), 890–902. doi:10.1016/j.ijrmms.2007.01.005

Reyes, O., and Einstein, H. H. (1991). "Failure mechanisms of fractured rock - a fracture coalescence model," in *7th ISRM congress.* (United States: OSTI).

Shen, B., Stephansson, O., Einstein, H. H., and Ghahreman, B. (1995). Coalescence of fractures under shear stresses in experiments. *J. Geophys. Res. Solid Earth* 100 (B4), 5975–5990. doi:10.1029/95jb00040

Shen, B., and Stephansson, O. (1993). Numerical analysis of mixed mode I and Mode II fracture propagation. *Int. J. Rock Mech. Min. Sci. Geomechanics Abstr.* 30 (7), 861–867. doi:10.1016/0148-9062(93)90037-E

Shen, B. T., Sun, X. Z., Yin, D. W., and Li, Y. Y. (2022). Experimental study of the crack propagation and acoustic emission characteristics of red sandstone under cyclic loading. *GEOTECHNICAL Test. J.* 45 (3), 20190007. doi:10.1520/GTJ20190007

Song, D. Z., You, Q. J., Wang, E. Y., Song, X. Y., Li, Z. H., Qiu, L. M., et al. (2019). Characteristics of EMR emitted by coal and rock with prefabricated cracks under uniaxial compression. *GEOMECHANICS Eng.* 19 (1), 49–60. doi:10.12989/gae.2019.19.1.049

Tham, L. G., Liu, H., Tang, C. A., Lee, P. K. K., and Tsui, Y. (2005). On tension failure of 2-D rock specimens and associated acoustic emission. *Rock Mech. Rock Eng.* 38 (1), 1–19. doi:10.1007/s00603-004-0031-6

Tiwari, R. P., and Rao, K. S. (2006). Post failure behaviour of a rock mass under the influence of triaxial and true triaxial confinement. *Eng. Geol.* 84 (3), 112–129. doi:10.1016/j.enggeo.2006.01.001

Wang, K. Z., Zhang, C., Gao, Y. H., Chen, H. J., and Xie, T. (2023). Influence of prefabricated fissure combinations on strength and failure characteristics of rock-like specimens under uniaxial compression. *Int. J. GEOMECHANICS* 23 (2), 2637. doi:10.1061/(ASCE)GM.1943-5622.0002637

Wang, M., Li, X., Yang, S., Teng, L., Chen, Q., and Jiang, S. (2022). Research on deformation and fracture characteristics of the fractured rock mass under coupling of heavy rainfall infiltration and mining unloading. *Front. Earth Sci.* 9, 792038. doi:10.3389/feart.2021.792038

Wang, S. Y., Sloan, S. W., Sheng, D. C., Yang, S. Q., and Tang, C. A. (2014). Numerical study of failure behaviour of pre-cracked rock specimens under conventional triaxial compression. *Int. J. Solids Struct.* 51 (5), 1132–1148. doi:10.1016/j.ijsolstr.2013.12.012

Wong, L. N. Y., and Einstein, H. H. (2009a). Crack coalescence in molded gypsum and carrara marble: part 1. Macroscopic observations and interpretation. *Rock Mech. Rock Eng.* 42 (3), 475–511. doi:10.1007/s00603-008-0002-4

Wong, L. N. Y., and Einstein, H. H. (2009b). Systematic evaluation of cracking behavior in specimens containing single flaws under uniaxial compression. *Int. J. Rock Mech. Min. Sci.* 46 (2), 239–249. doi:10.1016/j.ijrmms.2008.03.006

Wong, R. H. C., and Chau, K. T. (1998). Crack coalescence in a rock-like material containing two cracks. *Int. J. Rock Mech. Min. Sci.* 35 (2), 147–164. doi:10.1016/S0148-9062(97)00303-3

Wong, R. H. C., Chau, K. T., Tang, C. A., and Lin, P. (2001a). Analysis of crack coalescence in rock-like materials containing three flaws—Part I: experimental approach. *Int. J. Rock Mech. Min. Sci.* 38 (7), 909–924. doi:10.1016/s1365-1609(01)00064-8

Wong, R. H. C., Guo, Y. S. H., Li, L. Y., Chau, K. T., Zhu, W. S., and Li, S. C. (2018). "Anti-wing crack growth from surface flaw in real rock under uniaxial compression," in *Fracture of nano and engineering materials and structures*. Editor E. E. Gdoutos (Netherlands: Springer Netherlands), 825–826.

Wong, R. H. C., Huang, M. L., Jiao, M. R., Tang, C. A., and Zhu, W. S. (2004a). The mechanisms of crack propagation from surface 3-D fracture under uniaxial compression. *Key Eng. Mater.* 261-263, 219–224. doi:10.4028/www.scientific.net/KEM.261-263.219

Wong, R. H. C., Law, C. M., Chau, K. T., and Zhu, W. S. (2004b). Crack propagation from 3-D surface fractures in PMMA and marble specimens under uniaxial compression. *Int. J. Rock Mech. Min. Sci.* 41, 37–42. doi:10.1016/j.ijrmms.2004.03.016

Wong, R. H. C., Leung, W. L., and Wang, S. W. (2001b). "Shear strength studies on rock-like models containing arrayed open joints," in *DC rocks 2001, the 38th U.S. Symposium on rock mechanics (USRMS)* (Washington, D.C: USRMS).

Wong, R. H. C., Lin, P., and Tang, C. A. (2006b). Experimental and numerical study on splitting failure of brittle solids containing single pore under uniaxial compression. *Mech. Mater.* 38 (1), 142–159. doi:10.1016/j.mechmat.2005.05.017

Worley, R., Dewoolkar, M. M., Xia, T., Farrell, R., Orfeo, D., Burns, D., et al. (2019). Acoustic emission sensing for crack monitoring in prefabricated and prestressed reinforced concrete bridge girders. *J. BRIDGE Eng.* 24 (4), 1377. doi:10.1061/(ASCE)BE.1943-5592.0001377

Xi, X., Wu, X., Guo, Q. F., and Cai, M. F. (2020). Experimental investigation and numerical simulation on the crack initiation and propagation of rock with pre-existing cracks. *IEEE ACCESS* 8, 129636–129644. doi:10.1109/ACCESS.2020.3009230

Xiao, N., Luo, L. C., Huang, F., and Ling, T. H. (2022). Numerical study of rock mechanical and fracture property based on CT images. *GEOMECHANICS Eng.* 31 (4), 395–407. doi:10.12989/gae.2022.31.4.395

Xu, N. Z., Liu, C. Q., Wang, Y. J., Dang, H. B., and Ma, D. (2021). Biaxial shear crack propagation modes of rock-like specimens with prefabricated fissures and their strength characteristics. *Shock Vib.* 2021, 1–12. doi:10.1155/2021/7248926

Yang, S. Q., and Jing, H. W. (2010). Strength failure and crack coalescence behavior of brittle sandstone samples containing a single fissure under uniaxial compression. *Int. J. Fract.* 168 (2), 227–250. doi:10.1007/s10704-010-9576-4

Yang, S., and Jiang, Y. (2010). Triaxial mechanical creep behavior of sandstone. *Min. Sci. Technol. (China)* 20 (3), 339–349. doi:10.1016/s1674-5264(09)60206-4

Yang, S. Q., Yang, D. S., Jing, H. W., Li, Y. H., and Wang, S. Y. (2012). An experimental study of the fracture coalescence behaviour of brittle sandstone specimens containing three fissures. *Rock Mech. Rock Eng.* 45 (4), 563–582. doi:10.1007/s00603-011-0206-x

Zhang, G., Chen, G., Xu, Z., Yang, Y., and Lin, Z. (2020). Crack failure characteristics of different rocks under the action of frost heaving of fissure water. *Front. Earth Sci.* 8, 13. doi:10.3389/feart.2020.00013

Zhang, S., Wang, L. F., and Gao, M. Z. (2019). Numerical simulation of the influence of width of a prefabricated crack on the dimensionless stress intensity factor of notched semi-circular bend specimens. *SHOCK Vib.* 2019, 1–10. doi:10.1155/2019/3291730